High resolution CO observations of S88-B

Astron. Astrophys. 266, 452–456 (1992)

ASTRONOMY AND ASTROPHYSICS

High resolution CO observations of S88-B

G.J. White[1] **and C.V.M. Fridlund**[2]

[1] Department of Physics, Queen Mary and Westfield College, University of London, Mile End Road, London E1 4NS, England
[2] Astrophysics Division, Space Science Department, ESTEC, Postbox 299, NL-2200AG, Noordwijk, The Netherlands

Received April 6, accepted July 12, 1992

Abstract. CO J=2-1 and ^{13}CO J = 2-1 and 1-0 observations have been made of the HII region S88-B using the 15m James Clerk Maxwell telescope in Hawaii, and the 20m telescope at Onsala. The core of the cloud is resolved into a horseshoe-like structure which surrounds a diffuse reflection nebula. The central core has a mass of $\geq$ 1000 $M_\odot$, with 400 $M_\odot$ in the horseshoe structure. The gas in the horseshoe appears highly fragmented, and has a kinetic temperature of $\approx$ 60 K, suggesting it is closely coupled to the dust temperature. A recently formed high mass star appears to be in the process of evacuating a cavity, possibly through a large molecular outflow that is found to show an accelerated component in its blue-shifted lobe. A velocity gradient across the horseshoe structure suggest ordered motion, and could represent rotation in the parental cloud.

Key words: stars: formation of – interstellar medium: clouds: S88 – interstellar medium: HII regions: S88-B – radio lines: molecular

1. Introduction

The evolved HII region S88 is a low emission-measure nebula, which contains at least one site of high mass star formation. The radio continuum structure has been studied by Felli & Harten (1981), who detected radio emission from two regions, S88-A, and S88-B, located SE of S88 proper. The more easterly component of these, S88-B, lies behind up to 40 magnitudes of visual extinction. This region is further resolved into two compact HII regions, S88-B1 and S88-B2. The latter component is an extremely high emission measure, and very deeply embedded, object. About 40 arc seconds southwest of this radio knot a nebulous region with a diameter of $\approx$ 50 arc seconds and showing strong Hα emission is seen.

The molecular cloud associated with S88 has been studied in CO (Evans et al. 1981, Phillips et al. 1988 and Phillips & Mampaso, 1991). The infrared emission from S88A and B was also mapped by Evans et al. (1981), who found extended far-infrared emission centered on the compact HII regions S88-B1 and -2. At near-infrared wavelengths , the peak emission is shifted towards the Hα nebulosity indicating a high degree of extinction towards the ionizing sources. The far-infrared spectrum of the S88-B complex was found to be consistent with a dust temperature of 48 K. The inferred infrared luminosity is 1.8 x 10^5 $L_\odot$, thus indicating the high mass nature of star formation in this region.

Send offprint requests to: C.V.M. Fridlund

The absence of significant 2mm H_2CO emission in the data of Evans et al. (1981) imply that the core density is less than 10^5 cm^{-3}. This is low for a high mass star formation region, but is nevertheless consistent with modelling of CO lines by Phillips et al. (1988, 1991) who estimate the density to be a few x 10^4 cm^{-3}.

From low angular resolution observations with the United Kingdom Infrared Telescope (UKIRT) in the CO J=2-1 and 3-2 transitions, a velocity gradient running NE-SW across at least the central 4 arcminutes of the cloud core was found, suggesting large scale rotation (Phillips et al 1988, 1991). These author also found evidence for a spatial separation of the high velocity blue and red shifted gas.

The morphology of this outflow appears quite different from that of other molecular outflow sources, in that the reported blue-shifted high velocity emission lies towards the more heavily extinguished part of the cloud, whilst the red-shifted gas is found close to the position of the Hα emitting nebulosity and thus presumably at the front of the cloud.

In order to study this object at higher angular resolution, and to help understand the kinematic and density structure, we have made well sampled maps in the CO J=2-1 and ^{13}CO J=1-0 and 2-1 transitions.

2. Observations

For the CO & ^{13}CO J=2-1 data we used the 15m James Clerk Maxwell Telescope (JCMT) in Hawaii. We used a cooled mixer system (White 1988) with a digital autocorrelation spectrometer with a bandwidth of 128 MHz. For the ^{13}CO observations the backend was an AOS with a bandwidth of 500 MHz instead. Calibration was obtained frequently by measurement of the sky brightness temperature, and ambient and cold loads. The zenith sky temperature was typically 10-15 K, and the single-sideband system noise temperature was $\approx$ 1000 K. All spectra have been calibrated to a scale of T_R^*, and offsets are relative to the adopted (0,0) position at RA (1950) = 19^h 44^m $42^s.5$, Dec (1950) = + 25^o 05' 30".

For the ^{13}CO J=1-0 spectra we utilized the 20m Onsala telescope, Sweden, equipped with a Schottky diode mixer having a single-sideband noise temperature of $\approx$ 450 - 500K on the sky [1]. This telescope was operated in a position switching mode, using a 256 channel filter bank of 250 kHz resolution. These observations

[1]The Onsala Space Observatory is operated by the Research Laboratory of Electronics, Chalmers University of Technology, Göteborg, Sweden, with financial support from the Swedish Natural Research Council (NFR) and the Swedish Board for Technical Developement

Table 1. Log of observations

Species	Date	ΔV (km s^{-1})	Beam (")	Pointing (")	η_{fss}	Grid spacing (")	No. of spectra
CO J=2-1	August 1987	0.95	22	$\lesssim 5$	0.73	14	162
^{13}CO J=2-1	June 1989	0.45	22	$\lesssim 5$	0.75	14	98
^{13}CO J=1-0	July 1988	0.68	33	$\lesssim 5$	0.68	15/30	54

were also calibrated to a scale of T_R^*. More information about the observations can be found in Table 1.

3. Results

The CO J=2-1 data is displayed in Figure 1, where in a) we show a map of the maximum T_R^*. The CO shows a horseshoe-like distribution, with its temperature peak lying approximately at the interface between the optically visible nebulosity and the position of S88-B1 (Felli & Harten, 1981), where T_R^* is $\approx$ 56 K, similar to the dust temperature estimated by Evans et al. (1981) from far-infrared data. The two 'legs' of the horseshoe extend up to 2 arcminutes southwards; a secondary peak in the western 'leg' with $T_R^* \approx 47$ K is coincident with IRS-5, an embedded near-infrared point source (Evans et al. 1981). The CO J=2-1 emission surrounds the Hα nebulosity, which becomes visible where the CO intensity drops off rapidly. The lowest value of peak T_R^* is coincident with the maximum Hα emission seen in the images of Deharveng & Maucherat (1978).

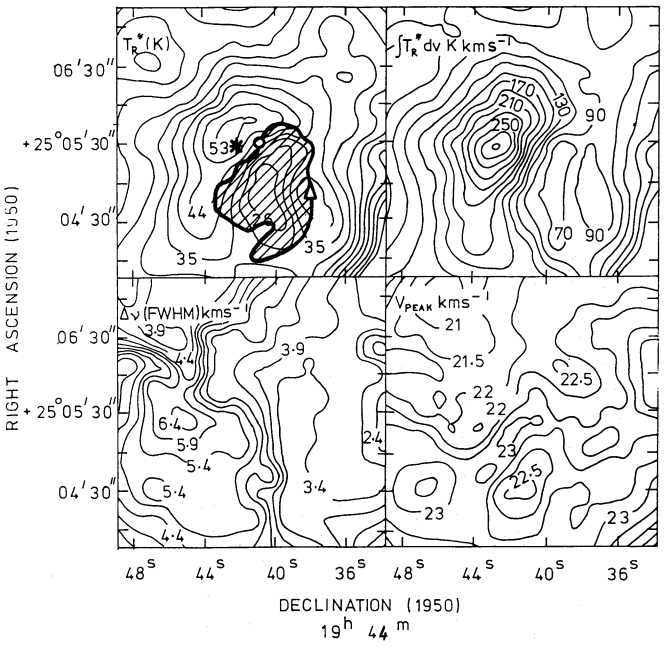

Fig. 1. Maps in the CO J = 2-1; a) peak antenna temperature (K), b) integrated antenna temperature (K km s^{-1}), c) linewidths (km s^{-1}) and d) the velocity of the line peak (km s^{-1}). In panel a), the asterism represents the HII emission peak (B2). The circle and triangle are IR sources P & 5 respectively, in Evans et al .'s study (1981). The shaded area represents the visible nebulosity

In Figure 1b, the map of integrated CO J = 2-1 emission shows a similar horseshoe-like structure, but it is less symmetric than the map of T_R^*, has a more pronounced peak close to the compact HII regions, and is weaker towards the western 'leg' of the horseshoe. One reason for this can be seen in Figure 1c, which shows the linewidth. The maximum line-widths are found $\approx$ 45 arcseconds east of the (0,0) position, and narrow markedly across the Hα region. The individual spectra show that there are at least two separate velocity components at velocities of $\approx$ 21 - 22 km s^{-1} and 24 - 25 km s^{-1}, as well as other emission extending over the velocity range 13 - 30 km s^{-1}. In Figure 1d, the velocity of the peak antenna temperature across the map is shown. A velocity gradient of $\approx$ 1 km s^{-1} arcmin^{-1} is running from the northeast towards the southwest. This velocity gradient was detected by Phillips et al. (1988) in low spatial resolution CO J=2-1 & J=3-2 observations, and they suggested that it was caused by the ambient cloud undergoing slow rotation. The interpretation is ambiguous since the kinematic structure show multiple velocity components (self-absorbed) in the spectra. What can be said from our present observations, however, is that we have indications of an ordered structure in the data. Whether this is caused by a velocity change of emission components, or a gradient in absorption components will have to be determined by future observations.

In Figure 2, CO J = 2-1 maps are shown for individual velocity channels.

At the most blueshifted velocities between 13 and 16 km s^{-1}, the emission is appearing at the northern edge of our map, and moves southwards as we proceeds towards lower velocities relative to the ambient cloud velocity. At 18 km s^{-1}, the dominant emission is emanating from the position (+25,0), close to S88-B1 and S88-B2. At 18 and 19 km s^{-1}, two compact emitting regions are visible at (-35,-50) and at (55,-50). Between 19 and 21 km s^{-1}, the eastern leg of the horseshoe becomes stronger, and emission along the western edge of the Hα region can be seen. At velocities redshifted from the central cloud velocity, the western leg of the horseshoe becomes more prominent, peaking at $\approx$ 23 km s^{-1}. Between 23 and 24 km s^{-1}, the CO depression close to the optical region is most pronounced. The horseshoe structure can be traced out to a velocity of $\approx$ 25 km s^{-1}, where it separates into two individual peaks. At the highest red-shifted velocities emission is seen close to the Hα maximum, and towards the south of our map.

The ^{13}CO J=2-1 data show the same basic morphology as the CO maps. In particular the considerable amount of fragmented structure is visible also in this isotope. The main difference between the two transitions occurs in the SE edge of the horseshoe, where the ^{13}CO/CO line ratios are higher. The ^{13}CO emission adjacent to the ionised gas shows a more rapid fall off in intensity than seen in the CO data.

The ^{13}CO J=1-0 data (individual velocity channel maps in Figure 3) has a broadly similar distribution to that displayed by the ^{13}CO J=2-1 data, with peak values of $T_R^* \approx$ 14K being seen at the offset (+15,-15). The linewidths of the ^{13}CO J=1-0 lines vary from 1.8 to 4.3 km s^{-1}, with the broadest lines being seen close to the ^{13}CO peak. Towards several positions, particularly in the northeast, the ^{13}CO lines exhibit a blue wing seen to $\approx$ 13 km s^{-1} in individual spectra. In the southeast the line separates into two velocity components at 19 km s^{-1} and 21 km s^{-1} –

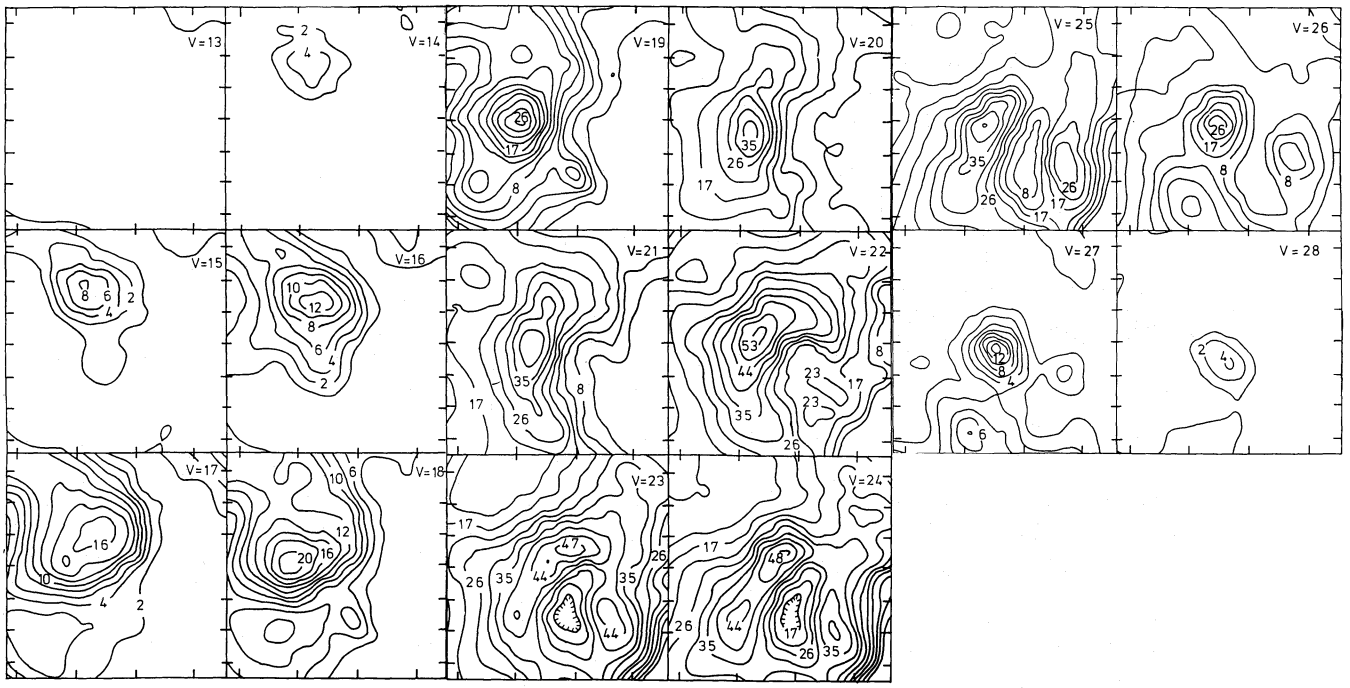

Fig. 2. Maps of the antenna temperature (in units of T_R^*), integrated in individual 1 km s^{-1} velocity channels. The scales are as in Fig. 1

something which can also be seen in the individual CO J=2-1 spectra.

4. Discussion

The structure of the region at low velocities relative to that of the ambient cloud, is dominated by the horseshoe-like distribution of molecular material surrounding the Hα emission nebula. The material in the horseshoe gives a fragmented impression, with different maxima separated by 1 – 2 km s^{-1} or more, and with a size scale of ≈ 30 arcsec or larger.

The highest kinetic temperature, T_K, of the molecular gas, based on the strongest CO lines, is ≈ 58K (assuming optically thick CO). This agrees well with the dust temperature, T_D, as determined by Evans et al (1981) from mid- and far- infrared observations, and given the uncertainties in the two determinations. These values are, however, considerably higher than the estimate of T_K reported recently by Wu & Evans (1989) based on CO J=1-0 data (≈ 35K with a beamsize of 2.3 arc minutes) and using the ratio of the long wavelength channels intensities from the IRAS Point Source Catalogue (≈ 38K with an effective beamsize ≈ 4 arc minutes). Since the present data have higher resolution than these other studies, we have convolved our data to the 2.3 arc minute resolution of the J=1-0 observations, which reduces our estimate of T_K to 35K, bringing it into excellent agreement with Wu and Evans (1989) and the CO J=2-1 data of Phillips et al (1988). This suggests that the dust and gas temperatures are closely coupled together. We have re-examined the anomalous position reported by Evans et al (1981) to show T_K greater than T_D by 13K, and we find $T_K \geq 28/\eta_c$ K. Since $\eta_c \approx$ unity, $T_D \geq T_K$, relaxing the problem discussed by Evans et al (1981) which led them to suggest breakdown of the Goldreich & Kwan (1974) hot dust-cool gas model as applied to S88.

For optically thin conditions the ratio of of the ^{13}CO J=2-1 and 1-0 lines will be given by:

$$\frac{T_R(^{13}CO(J=2-1))}{T_R(^{13}CO(J=1-0))} \approx 4 \times e^{\left(\frac{-10.6}{T_{ex}}\right)} \qquad (1)$$

This ratio is ≈ 3 for T_{ex} between 25K and 100K. For optically thick emission, the ratio will instead be close to unity. Taking the measured J=1-0 and 2-1 ^{13}CO lines intensities, and dividing by η_c, the coupling efficiency to a 50 arc second diameter (typical FWHM of most prominent features in our data) gaussian source (assumed to be 0.8 and 0.95 respectively), the data are found to be consistent with the optically thin limit within the calibration uncertainties.

The CO profiles are generally complex, containing wings and apparent self-absorbed components. Despite this complexity, the CO and ^{13}CO J=2-1 data can be used to make a first order lower limit estimate of the molecular hydrogen column density towards S88-B, N_{tot}, where

$$N_{tot} \approx \frac{6 \times 10^{19}\left(1+\frac{0.87}{T_{ex}}\right) \times \tau_{13} \times \frac{T_R^*}{\eta_c} \times dV}{\left(1-e^{\left(-\frac{10.6}{T_{ex}}\right)}\right) \times \left(e^{\left(-\frac{5.3}{T_{ex}}\right)}\right) \times (1-e^{-\tau_{13}})} cm^{-2} \qquad (2)$$

Here T_R^* is the intensity of the J=2-1 ^{13}CO line, T_{ex} is the excitation temperature, η_c is the source coupling efficiency, τ^{13} is the ^{13}CO optical depth, and additionally assuming a relative abundance ratio $[H_2]/[^{13}CO] = 5 \times 10^5$.

Using this relationship, the lower limit to the total mass in the area covered by the ^{13}CO J=2-1 observations is ≈ 1300 $M_\odot$, about double that estimated by Evans et al (1981). This probably reflects the higher resolution of our data, resulting in a more adequate beam filling factor for a clumpy medium. The lower limit to the mass contained in the horseshoe is ≈ 400 $M_\odot$.

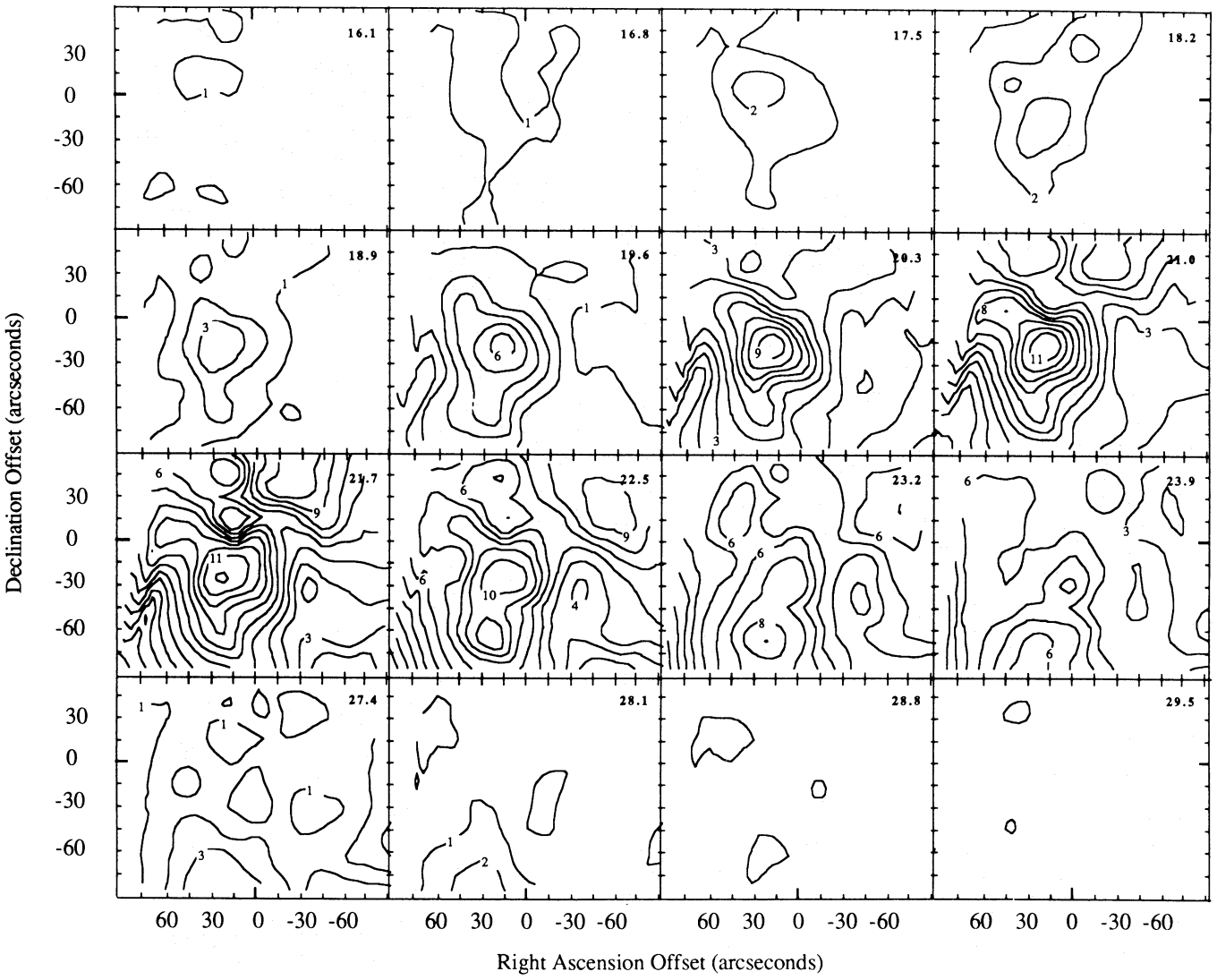

Fig. 3. Maps of T_R^* in the ^{13}CO J = 1-0 line for 1 km s^{-1} velocity channels. The lowest contour is at T_R^* = 1K, and incrementing by 1K. The offsets are in arc seconds from the (0,0) position

In order to construct a model for S88-B, it is useful to compare our data with Figures 17 – 19 of Phillips & Mampaso (1991, hereafter PM). One can immediately see that their maps of T_R^*, ΔV (FWHM) and V_{peak} are similar to ours, but our data covers a larger area, and shows the horseshoe character which is not evident in their observations. PM have integrated their CO, J = 2–1 observations between $\approx$ 16 and -4 km s^{-1} (blue) and $\approx$ 25 and 45 km s^{-1} (red) – that is, well outside what the S/N of our corresponding data allows us to do – in order to study the wing emission. The resulting map (their Figure 19) shows a well defined red emission lobe superposed on the position of the Hα emission, as well as another area of 'red' emission one arcmin south (to facilitate the discussion we will call these the North Red Lobe, NRL, and the South Red Lobe, SRL). A blue emission lobe (BL) is clearly seen towards the north of S88-B. PM interpret their data as supportive of a low-collimation bipolar outflow, a conclusion already tentatively reached by Phillips et al.(1988). All three features noted by PM are clearly discernable at the extreme velocities in our Figure 2. Both areas of 'red' emission are visible between 26 and 28 km s^{-1}. The blue lobe is visible between 13 and 17 km s^{-1}, and it is shifted progressively closer towards the horseshoe structure as we proceed towards higher ('redder') velocities. This implies an outflow with acceleration along the major axis, such as e.g. L1551 (Fridlund et al., 1984, 1989) or Mon R2 (Meyers-Rice & Lada, 1991). In this picture, the SRL could either be part of the NRL and separated only by perspective. We note, however, that the two features visible in Figure 2 at (-35,-50) and (55,-50) and which have velocities between 18 and 19 km s^{-1} could be the 'blue' counterparts to the SRL if it is a bipolar outflow in its own right. The SRL as seen at 26 km s^{-1} in Figure 2 appears also to be more connected to the south east 'leg' of the horsshoe, as does indeed the 'blue' feature at (55,-50), than it does to the NRL. Our data can not separate this hypothesis from the one in which these two features are 'clumps' physically separated from the horseshoe structure, and high spatial/spectral resolution data with high S/N is needed to possibly resolve this issue.

The model that emerges, is that the horseshoe morphology is due to material excited along the periphery of an outflow cavity, inside of which the Hα region fits. Some of the heating of the molecular gas must be due to the embedded objects, but no obvious candidate can be found in the IR-maps of Evans et al. (1981) for some of the emission peaks in the horseshoe. In the western 'leg' Evans et al.'s near-infrared source No. 5 is a possible candidate but no far-infrared emission peaks are seen at this position. Additional energy, such as that available from photoelectric heating or shocks caused by the outflow, could be required to explain the temperature distribution which is seen. The rather limited available body of data on S88 is insufficient to allow qualitative discrimination between alternatives at the present time.

The position of the peak CO & ^{13}CO emission, lying very close to S88-B2 (the high emission measure component) suggest the formation of a high mass star at the edge of the cloud core. Immediately to the west of this, a cavity has been formed in the surrounding molecular cloud. Since the NRL is well centered on the optical nebulosity, it is possible that this cavity has been eroded out of the cloud mechanically. Radiative effects, however, can not be excluded due to the presence of at least one newly formed high mass star in the vicinity. This results in a geometrical configuration similar to that suggested by Evans et al. (1981). The near-IR peak, then results from UV heating of the gas along the opening which joins the edge of the cloud to the ionised outflow / reflection nebula.

5. Conclusions

1. The core of the S88 molecular cloud has been resolved into a horseshoe structure surrounding a small optical nebula. The main molecular condensation is associated with the deeply embedded compact HII region, S88-B2, although several other emission peaks are also visible within the horseshoe.
2. The total mass of the mapped region is of the order $\geq$ 1000 $M_\odot$, with $\geq$ 400 $M_\odot$ in the horseshoe structure.
3. The gas temperature reaches about 60K suggesting a close coupling to the dust temperature.
4. S88B appears to be an example of a high mass star forming in a moderate to low density region, and a cavity has been evacuated in the molecular cloud. The most likely source of this cavity is probably the red lobe of the molecular outflow associated with the core. The blue-shifted lobe appears to show an accelerated component in the northward direction.

We stress again, that the fine structure is complex, and it is possible that one or several more outflows are associated with the emission peaks in the horseshoe structure. More sensitive observations are needed to clarify this issue.

Acknowledgements. The CO observations were obtained during part of the Scientific Commissioning phase of the JCMT. We also wish to thank R. Booth, Onsala for the allocation of Summer Observing time during which the ^{13}CO J=1-0 observations were made. GJW wishes to thank Professors M. Morimoto and N. Kaifu and the staff of the Nobeyama Radio Observatory, for their hospitality, when initial processing of the S88 data was carried out. We also wish to acknowledge the comments of an anonymous referee, which resulted in a stricter structure of the paper.

References

Deharveng, L., Maucherat, M., 1978., A&A 70, 19
Evans, N.J.E., Blair, G.N., Harvey, P., Israel, F., Peters, W.L., Scholtes, M., de Graauw, Th., Vanden Bout, P. 1981, ApJ, 250, 200
Felli, M., Harten, R.H., 1981, A&A, 100, 42
Fridlund C.V.M.,Sandqvist Aa.,Nordh H.L., Olofsson G., 1984, A&A, 137, L17
Fridlund, C.V.M., Sandqvist, Aa., Nordh, H.L., Olofsson, G., 1989, A&A, 213, 310
Goldreich, P. and Kwan, J. 1974, ApJ 189, 441
Meyers-Rice, B.A., Lada, C.J. 1991, ApJ, 368, 445
Phillips, J.P., White, G.J., Rainey, R., Avery, L.W., Richardson, K.J., Griffin, M., Cronin, N.J., Monteiro, T. & Hilton, J. 1988, A&A, 190, 289
Phillips, J.P. and Mampaso, A. 1991, A&AS, 88, 189
White, G.J., 1988. 'Millimetre & Submillimetre Astronomy', p 27, Kluwer Academic Publishers, ed. R.D.Wolstencroft & W.B.Burton
Wu, Y. and Evans, N.J. 1989, ApJ, 340, 307.

This article was processed by the author using Springer-Verlag LaTeX A&A style file 1990.